2011 American Control Conference
on O'Farrell Street, San Francisco, CA, USA
June 29 - July 01, 2011

Cycle-to-cycle Estimation and Control of Multiple Pulse Profiles for a Piezoelectric Fuel Injector

Chris A. Satkoski, Neha S. Ruikar, Scott D. Biggs and Gregory M. Shaver

Abstract— **While common-rail diesel fuel injection systems utilizing solenoid-actuated injectors have drastically improved the ability to lower emissions, noise, and fuel consumption, their limited bandwidth does not allow for tightly spaced injections or rate shaping. Piezoelectric injectors have that capability, but introduce multiple control challenges that can compromise their improved functionality. This paper summarizes the use of estimation algorithms for cycle-to-cycle determination of an injection flow profile capable of being used as feedback for a closed-loop control algorithm. While the estimation equations are complex and require a small time step, the authors propose capturing important estimation feedback during the injection period and delaying the integration of state variables across the engine cycle to more efficiently utilize a real-time processor. Also, a simplified model is developed to represent the dynamics of simultaneously controlling the quantity of pulses as well as the realized dwell time in between pulses. The model accounts for the coupling between the two, and a control law is developed and refined to provide an overdamped response of both the pulse quantities and realized dwell time, in order to prevent pulse bleeding. Transient response of the controller is shown in simulation and validated with experimental data with good correlation.**

I. INTRODUCTION

Major advances in diesel combustion have come from the addition of common-rail, solenoid-actuated fuel injection systems. Independent control of injection pressure, timing, quantity and the number of pulses in a cycle has led to significant reductions in emissions such as nitrogen-oxides and particulate matter, as well as decreased noise and fuel consumption [1], [2].

Typically, electronic injectors meter fuel into the combustion chamber through the motion of an injector needle, which covers and uncovers the injector nozzles to start and stop flow. Solenoid actuators are generally not directly connected to the needle, but instead control a hydraulic circuit which redirects high pressure fuel across a portion of the needle to move it vertically. This technique does not allow tight spacing between pulses and therefore limits the number of injections per cycle.

Piezoelectric stack actuators have a much higher bandwidth and when used in an injector can create sufficient force to *directly* move the needle. This improvement not only allows for the injection of chains of tightly spaced pulses, but also speeds needle opening [3], creating better air entrainment, spray development, and injection velocity [4].

While piezoelectric injectors have the ability to create these multiple pulse profiles, robust implementation in such a highly dynamic environment is challenging. Small changes in operating conditions, such as rail pressure, the commanded dwell time, and the size of previous pulses can cause a tightly spaced, multiple pulse profile to bleed into a single pulse, effectively canceling the benefits of the high powered actuator [5]. Without knowledge of when pulses will bleed together and when they will separate, an engine control module (ECM) would have difficulty reliably reproducing complex profiles in a constantly changing environment.

One solution is utilizing closed-loop control to constantly correct injector input signals to produce desired pulse trains. However, utilizing fuel flow sensors on a production engine is currently impractical and cost prohibitive. A more feasible solution is to create a dynamic observer which can accurately estimate a fuel profile, even complex, multiple pulse profiles. With an on-board estimate of injection rate shape, control strategies can be implemented to correct for variations in fueling due to environmental factors and optimize the capability of the piezoelectric actuated injector.

Previous work has shown effective model-based estimation of injection profiles [5] based on a physical simulation model of a particular style of piezoelectric fuel injector [6]. While this estimation strategy was validated off-line, closed-loop control will require fast computation of model states to achieve cycle-to-cycle control of injection. This paper summarizes the implementation of this previously developed estimation strategy in a real-time environment for cycle-to-cycle computation of flow rate. Also, a candidate controller is designed and tested to allow for cycle-to-cycle tracking of pulse quantity and realized dwell for a multiple pulse profile.

II. EXPERIMENTAL HARDWARE

This piezoelectric injector measurement and control rig at Purdue allows for accurate control of the injector driver as well as simultaneous high speed measurement and logging of critical signals through a dSPACE system. The simulated injection environment can be run at various speeds, but for the experiments shown here the measurements are taken at a 500 RPM cam speed (1000 RPM crank). The complete setup can be seen in Fig. 1. Subsystems of the rig are described below.

C. Satkoski is a Graduate Researcher in the Department of Mechanical Engineering, Herrick Labs, Purdue University, West Lafayette, IN casatkos@purdue.edu

N. Ruikar is an Graduate Researcher in the Department of Mechanical Engineering, Herrick Labs, Purdue University, West Lafayette, IN

S. Biggs is an Undergraduate Researcher in the Department of Mechanical Engineering, Herrick Labs, Purdue University, West Lafayette, IN

G. Shaver is with the Department of Mechanical Engineering, Herrick Labs, Purdue University, West Lafayette, IN

978-1-4577-0079-8/11/$26.00 ©2011 AACC

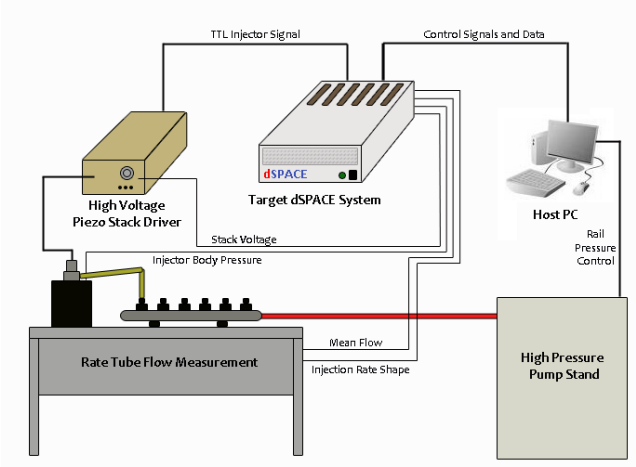

Fig. 1. Injector Measurement and Control Experimental Setup

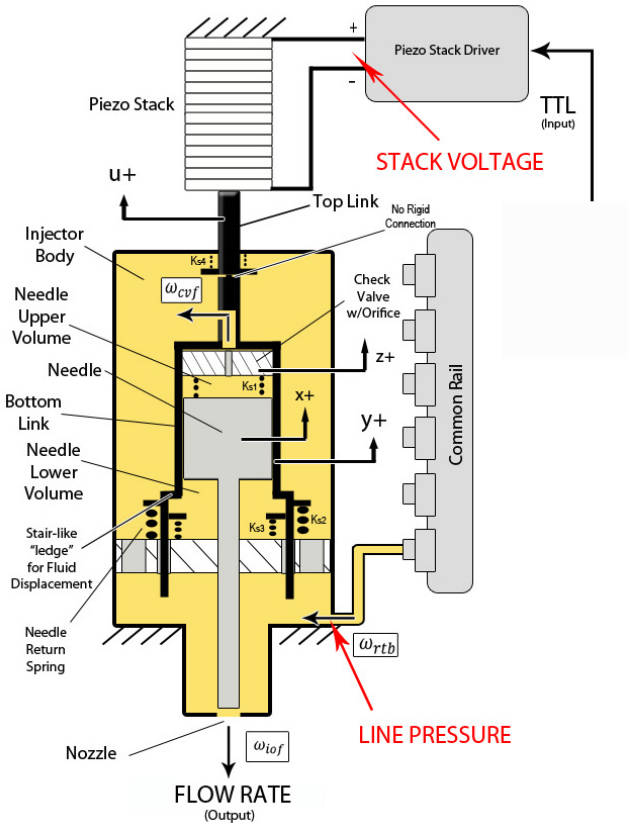

Fig. 2. Injector Schematic Representation

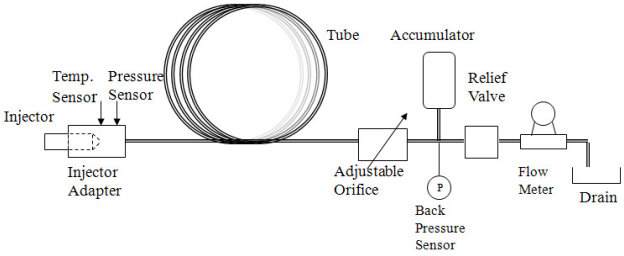

Fig. 3. Rate Tube Flow Measurement Principle

A. Injector

The injector used in this analysis is a prototype direct acting piezoelectric diesel fuel injector. A schematic representation of this injector's basic operating principle can be seen in Fig. 2.

When a TTL (Transistor-Transistor-Logic) signal is sent to the piezo stack driver the piezo stack is charged. This causes expansion of the piezo stack which pushes downward on the top and bottom link. The stair-like "ledge" is sized for hydraulic amplification of needle lift by displacing fluid in the needle lower volume. When this volume is pressurized, the needle is forced upward pushing fluid out of the needle upper volume through the check valve orifice into the injector body. The orifice is sized to control oscillation of a rapidly opening needle. When the stack is discharged, the process is reversed to close the needle. However, now a rapidly decreasing pressure in the needle upper volume can cause the check valve to open, allowing fluid to flow in faster which quickly closes the needle.

B. Flow Measurement - Benefits and Limitations

To validate the estimation and control algorithms outlined in the paper, injector flow must be measured. The fuel flow measurement device used in this analysis is based on the Bosch fuel rate indicator principle [7], also known as the rate tube measurement principle (as referenced in Fig. 1).

The details of the rate tube principle are shown in Fig. 3. The injector is secured in a fixture, which is connected to a long coiled tube. The tube is regulated to a pressure similar to that in a combustion chamber (approx. 70 bar). The coiled tube is sufficiently long to delay reflected pressure waves which bounce off the end of tube for a period of time which will prevent interference with the current measurement. A pressure sensor is placed at the tip of the injector. During injection, the pressure at the injector nozzle is roughly *proportional* to the injector flow rate. To accurately measure the quantity of the flow, a mean flow sensor is placed downstream in the low pressure segment of the system. This flow sensor is not high enough bandwidth for cycle-to-cycle measurements, and can take several cycles to converge to the mean flow through the system. For this reason, a large number of cycles are collected for a given operating point to allow the flow to converge. The mean flow is averaged over these cycles to approximate the quantity injected per stroke. The flow rate shape taken from the pressure sensor at the nozzle is averaged over those cycles and scaled such that integral under the curve matches the measured flow per stroke.

While this method has been shown to be a fairly reliable method of injection measurement, it does have some drawbacks. Pressure fluctuations in the system can cause unwanted noise. Also, because this takes multiple cycles to take a measurement of average flow rate, cycle-to-cycle

control strategies can only be validated before and after convergence of the flow. Intermediate flow quantities cannot be guaranteed, however, the shapes are accurate on a cycle-to-cycle basis.

C. Processing and Data Acquisition

Real-time processing, A/D conversion, and the creation of digital TTL signals is all done using a dSPACE system. Anti-aliasing filters are used for the pressure measurement in the rate tube system, as well as for an injector body pressure sensor. Both pressure sensors are piezoelectric. Critical devices utilized in the system are shown below in Table I.

TABLE I
DATA COLLECTION SYSTEM SPECIFICATIONS

FUNCTION	DEVICE
Processor	DS1005
A/D Conversion	DS2004
Digital I/O	CP4002
Anti-Aliasing Filter	KROHN-HITE 3364

The processor runs at a fundamental time step of 100 μs and A/D signals are buffered at 100 kHz (reference Sect. IV for more details). TTL signals are created directly using the digital CP4002 board for high resolution signals. The cutoff frequency of the anti-aliasing filter is set to 40 kHz.

III. Dynamic Estimation Structure

While this rig may have flow rate measurement capability, that will not be available when used in an actual engine. Therefore, a dynamic estimation of flow rate shape can be used to provide feedback to an on-line controller. The estimator used in this analysis is based on the following structure shown below in Fig. 4, described briefly below, but in detail in [5].

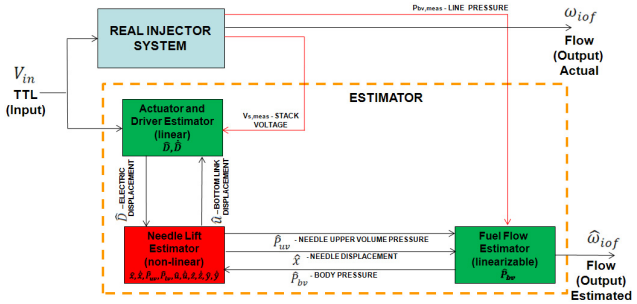

Fig. 4. Graphical Layout of Feedback Estimator [5]

The estimator includes a set of 13 non-linear dynamic equations, separated into sub-models. Each sub-model is separated into groups of related equations, which are dynamically coupled with other sub-models. The sub-models are the following:

- Actuator and Driver Sub-model
- Needle Lift Sub-model
- Fuel Flow Sub-model

The actuator and driver sub-model includes the dynamic equations associated with the piezo stack and the driver circuitry. The needle lift sub-model describes the internal hydro-mechanical dynamics from stack displacement down to needle lift. The fuel flow sub-model incorporates the dynamics from fuel flowing in from the rail to fuel flowing out of the injector.

The equations are grouped this way to allow the available feedback (piezo stack voltage and injector body pressure) to be applied to the relevant sub-model. This simplifies the design and implementation of two dynamic full-order estimators for each sub-model with feedback. Linearized forms of the models are used for design of the estimator dynamics, and the feedback is then applied to the original non-linear equations [5].

IV. Cycle-to-Cycle Estimation

With a sufficient dynamic estimation strategy, the equations and feedback signals can be loaded onto the dSPACE platform for real-time execution. Code is executed on a real-time processor by syncing the model time step with a real clock, and as long as all of the executions in one time step of the code can be computed in that amount of time, then real-time computation of states is possible.

The framework of fuel injection in a reciprocating engine gives a useful advantage for this type of calculation. While there are a significant number of estimator calculations that require a small time step, making real-time processing more difficult, a fuel injection event takes place on a time scale generally less than 10 ms. For an engine running at 1000 RPM crank speed (500 RPM cam), there are 120 ms in a cycle. Because there is a significant amount of time in a cycle where the processor has few critical processes, that dead time could be used to compute states for a short window earlier in the cycle when injection occurred. As long as A/D conversions can occur during injection at the desired "effective" time step, then real inputs and measurements can be used for estimation. While this is not real-time, it can be used for cycle-to-cycle computation of states.

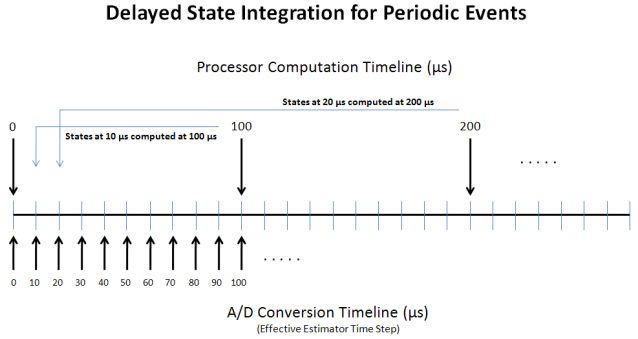

Fig. 5. Delayed Integration Technique for Cycle-to-Cycle Flow Rate Estimation

This computational strategy of "delaying" real-time integration is shown graphically below in Fig. 5. A/D conversions of necessary measurements (TTL signal, stack voltage, and body pressure) take place during a set window at the beginning of a cycle (approx. 10 ms). These values are stored in a temporary memory array for the duration of the cycle. A fundamental time step of 100 μs was found to be adequate for the real-time processor used here. Because the "effective" time step is 10 μs, at the first computational period of 100 μs the processor pulls the measurements stored at 10 μs and computes the states. This is repeated for each "effective" time step interval for the entire stored window.

Because computations takes place every 10 "effective" time steps, it takes 10 times longer than the event to calculate the states for the whole window. For example, if data is collected for the first 10 ms of an injection event, then it will take 100 ms to calculate the states for that entire window. For cycle-to-cycle control, the engine speed then cannot exceed 1200 RPM crank speed (600 RPM cam). Expanding the speed range can be done by increasing the "effective" model time step (at the expense of accuracy), reducing the real-time processor fundamental time step (may require model simplification), tightening the data collection window, allowing computations across multiple cycles, or using a faster processor. Fig. 6 shows an example pulse for a 1000 RPM crank speed cycle and the output for the estimator.

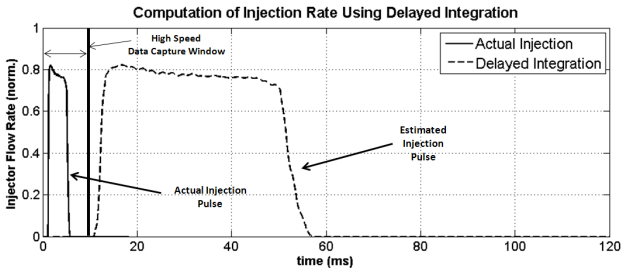

Fig. 6. Example of Delayed Time Integration for an Injection Pulse

Note that the injection event takes place during a relatively small portion of cycle (labeled "High Speed Data Capture Window"). The available measurements for estimating the flow rate (TTL signal, stack voltage, and body pressure) are captured and stored during this period at 10 μs intervals. Corresponding computations of estimator states are done at the processor interval of 100 μs using data stored in an array. This creates an estimated flow rate profile where the time domain is scaled by 10. Rescaling the time axis gives the estimate in the proper time domain and allows processing the profile as needed. This can be repeated every cycle allowing for cycle-to-cycle estimation of flow.

V. Cycle-to-Cycle Control

Once an estimated flow rate can be provided every cycle, a control strategy can be developed using the estimated profile as feedback. While there are a variety of control strategies possible, a common requirement for a flow profile would be specifying the following properties:

- Number of Pulses
- Quantity of Fueling in Each Pulse
- Realized Dwell Time in Between Pulses

Here realized dwell time refers to the actual dwell time in between two pulses (as opposed to the commanded dwell time in between TTL signals).

Previous work has shown that when pulses become tightly spaced, there are multiple external factors that can cause two separated pulses to bleed and become one. Variation in commanded dwell time (CDT), the size of a previous pulse, and the rail pressure can all cause two separated pulses to bleed into one [5]. If the full potential for the piezoelectric injector is to be utilized, creating tightly spaced, multiple pulse profiles will require knowledge of these interactions in order to make appropriate corrections.

This analysis will assume control is being done at a given rail pressure. Starting with two pulses, it is known that the quantity of the first pulse is directly impacted by the commanded on time (COT) of the TTL signal sent to the injector. It is also known that the realized dwell (RD) time in between the pulses is directly effected by the CDT. These variables can be seen graphically below in Fig. 7.

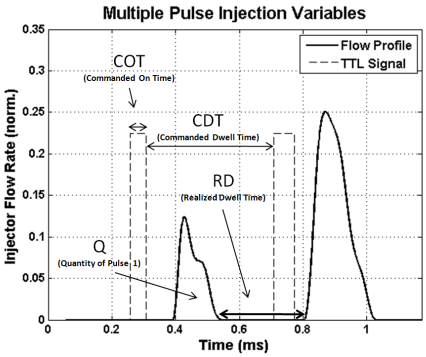

Fig. 7. Variables Used in Control of Multiple Pulse Profiles

A more subtle relationship between the first pulse and the realized dwell also exists, and becomes very important when pulses become tightly spaced. When the length of the COT of the first pulse is increased, this causes the maximum height of the injector needle to be higher, and subsequently take longer to close. For a given commanded dwell time, varying the size of the initial pulse can have a significant impact on the realized dwell time. This effect is represented in the Fig. 8.

For every profile shown in Fig. 8, the CDT between the pulses is the same, but the realized dwell time varies considerably. The continually increasing peak needle lift extends the delay between the first TTL pulse turning off and the needle closing. Note that this effect saturates once pulses are long enough that the peak needle lift is at its maximum. At this point, the time for the needle to close stays fairly constant regardless of how much longer the pulse stays on.

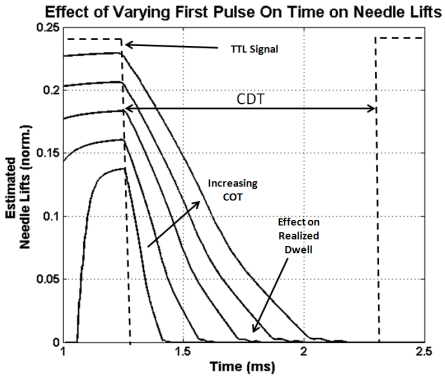

Fig. 8. Variation of Needle Lifts with First Pulse On Time

Because of the saturation, this effect is only significant for pulses which do not saturate the needle lift. However, any control action which simultaneously changes the size of the first pulse and the dwell time needs to account for this effect to be robust.

A. Two Pulse Appproximation

The COT of the first pulse and the CDT between the first and second pulses have a strong correlation to the first pulse quantity and the realized dwell (RD) between the pulses. However, this doesn't necessarily extrapolate to a series of pulses as there can be some effects that carry over to subsequent pulses (e.g. the needle not completely shutting prior to the onset of a subsequent pulse). To simplify the control design, this analysis will assume these effects are negligible and that series of multiple pulses can be separated into pairs of two pulses, each dynamically decoupled. This is a good assumption as along as a large enough dwell time is realized between pulses such that the system is "at rest" before the onset of the next pulse.

The quantity of pulse one is controlled by the first commanded on time. The second pulse quantity is controlled by the second on time. The RD between the first and second pulses depends on the COT for the first pulse and the CDT. This continues for as many pulses as there are in the series.

B. Model

Utilizing the two pulse approximation, the relevant modeling relationships can be determined. At a given rail pressure, the quantity Q of the first pulse is estimated well by a linear relationship to the commanded on time (COT), shown below in Eq. 1.

$$Q = \alpha \cdot COT \tag{1}$$

where α is the coefficient for a particular rail pressure. The RD is directly related to the CDT and also the COT for the first pulse for an unsaturated needle shown below in Eq. 2.

$$RD = \beta \cdot CDT - \phi \cdot COT \tag{2}$$

where β relates the CDT to the RD and ϕ approximates the change in RD as a result of increasing the size of the first pulse.

α is a constant which is unique (and proprietary) to a particular injector for a given rail pressure. Experimental data is used to determine a fit. For any given first pulse COT, a certain change in CDT generally leads to an equivalent change in RD, so for this model, β = 1. The relationship between COT and RD is complex, as seen in Fig. 8, and becomes constant once the injector needle saturates. Fig. 9 shows the effect of COT on RD at a constant CDT.

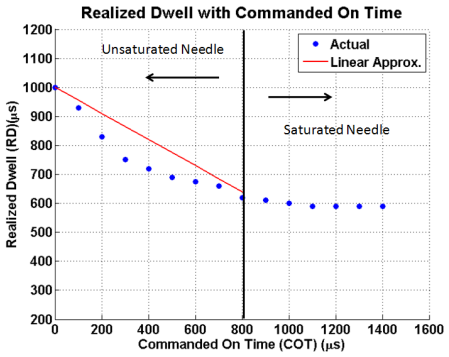

Fig. 9. Linear Approximation of RD with COT for an Unsaturated Needle

Fig. 9 shows how increasing COT eventually leads to needle saturation. Before saturation the effect is exponentially decaying, and a linear approximation created for the purpose of this control model is displayed. The slope of the linear approximation yields ϕ = 0.45.

These equations are valid for any given cycle, but are not dynamic. An instantaneous change in COT or CDT before a cycle leads to an instantaneous change in the quantity and realized dwell. This means that cycle-to-cycle dynamics will be dictated by the addition of some control action. A candidate controller could be the following modified discrete integral controller shown below in Eq. 3.

$$u(k+1) = u(k) + P \cdot e(k) \tag{3}$$

where u is the control input, P is a gain, e(k) is the control variable error, and k is the engine cycle. This is slightly different than a standard discrete integral controller which defines the current input based on a previous input and the current error. Using the control inputs of COT and CDT, discrete control laws can be created for both the pulse one quantity and realized dwell based on the estimated error shown below in Eq. 4 and 5.

$$COT(k+1) = COT(k) + P_1(Q_{des} - Q(k)) \tag{4}$$

$$CDT(k+1) = CDT(k) + P_2(RD_{des} - RD(k)) \tag{5}$$

where P_1 is the gain for the first pulse quantity controller and P_2 is the gain for the realized dwell controller. Q_{des} and RD_{des} are the desired first pulse quantity and realized dwell

time, respectively. Q(k) and RD(k) are the estimates acquired using the estimation strategy in Sect. III and [5]. Substituting Eq. 1 and Eq. 2 into Eq. 4 and 5 yields the following coupled discrete equations.

$$COT(k+1) = (1-P_1\alpha)COT(k) + P_1 Q_{des} \tag{6}$$

$$\begin{aligned} CDT(k+1) &= (1-P_2\beta)CDT(k) \\ &+ P_2 \cdot \phi COT(k) + P_2 RD_{des} \end{aligned} \tag{7}$$

Assigning x_1 = COT, x_2 = CDT, u_1= Q_{des}, u_2 = RD_{des}, a state space representation of the dynamics is shown below in Eq. 8.

$$\begin{bmatrix} x_1(k+1) \\ x_2(k+1) \end{bmatrix} = \begin{bmatrix} (1-P_1\alpha) & 0 \\ P_2\phi & (1-P_2\beta) \end{bmatrix} \begin{bmatrix} x_1(k) \\ x_2(k) \end{bmatrix} + \begin{bmatrix} P_1 & 0 \\ 0 & P_2 \end{bmatrix} \begin{bmatrix} u_1(k) \\ u_2(k) \end{bmatrix} \tag{8}$$

Because Q and RD are the variables to be controlled and can be estimated, they are defined as the outputs y_1 and y_2, respectively, shown below.

$$\begin{bmatrix} y_1(k) \\ y_2(k) \end{bmatrix} = \begin{bmatrix} \alpha & 0 \\ -\phi & \beta \end{bmatrix} \begin{bmatrix} x_1(k) \\ x_2(k) \end{bmatrix} \tag{9}$$

Because of the state matrix being in lower triangular form, the eigenvalues for this system are along the diagonal and control gains are found with following equations.

$$P_1 = \frac{(1-\xi_1)}{\alpha} \tag{10}$$

$$P_2 = \frac{(1-\xi_2)}{\beta} \tag{11}$$

where ξ_1 and ξ_2 are the desired eigenvalues for the closed-loop system. Note from Eq. 8 and 9 that the response of x_1 and y_1 is not dependent on x_2. This means that the quantity is decoupled from the dynamics of the realized dwell.

C. Performance Requirements

For both pulse one quantity and realized dwell, an over-damped, asymptotic transient response is desired. Overshoot of realized dwell is undesirable since this could cause pulses to bleed together when very small realized dwell times are required. If the pulses bleed, there is no way to quantify the realized dwell for values less than zero, and the detection algorithm which determines each pulses quantity and dwell time from the estimated flow profile cannot determine which measured pulses correspond to which desired pulse. Therefore, when the number of desired pulses does not equal the number of measured pulses, the system overrides *all* of the pulses dwell times farther and farther apart until the number of measured pulses equals the number of desired pulses, then the control action continues. If the realized dwell controller again overshoots, the system may continue to switch back and forth between the controller and the override diagnostic, preventing convergence of the system.

D. Transient Response

Because $|\xi| < 1$ is required for stability in a discrete system, and positive, real eigenvalues correspond to an overdamped transient response, both poles were initially set to 0.5. The response for both the pulse one quantity and the realized dwell is shown below in Fig. 10 and 11. The initial values and desired values were chosen to be far apart to better see the response.

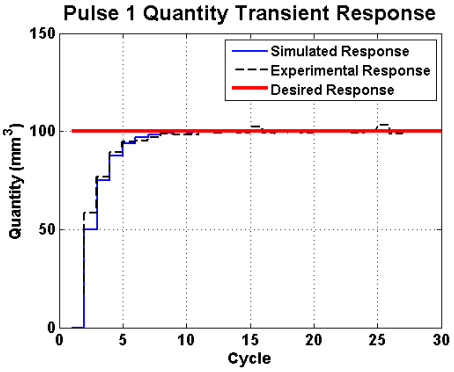

Fig. 10. Transient Response of Pulse One Quantity with Poles at 0.5

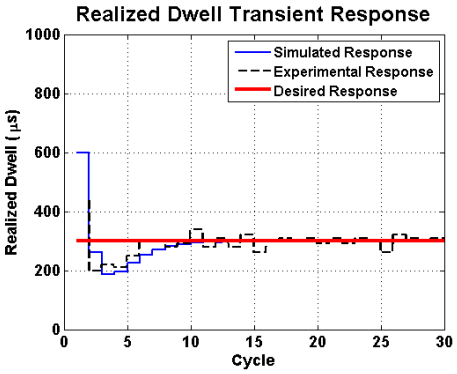

Fig. 11. Transient Response of Realized Dwell with Poles at 0.5

The pulse one quantity responded as expected with no overshoot. Even though both eigenvalues are positive and real, the realized dwell responded with fairly significant overshoot. To try and eliminate this overshoot, the second eigenvalue is slowed to 0.9. The first eigenvalue is left unchanged and the pulse one quantity plot is identical to Fig. 10. The realized dwell response with the slower eigenvalue is shown below in Fig. 12.

The response in Fig. 12 shows that even with a slower pole, overshoot still occurs. To understand this overshoot behavior, the state space formulation from Eq. 8 and 9 is converted to a discrete transfer function matrix through the conversion $\frac{Y(z)}{U(z)} = C(zI-A)^{-1}B+D$.

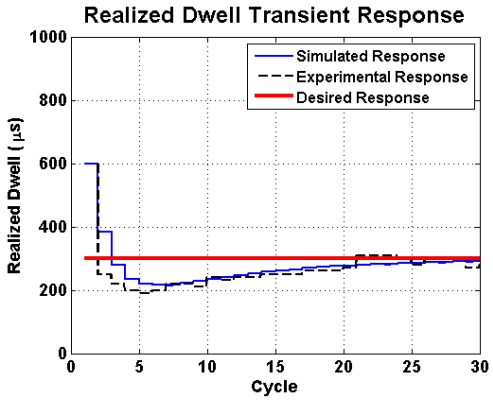

Fig. 12. Transient Response of Realized Dwell with Pole at 0.9

$$\begin{bmatrix} Y_1(z) \\ Y_2(z) \end{bmatrix} = \begin{bmatrix} \frac{\alpha \cdot P_1}{(z-(1-\alpha \cdot P_1))} & 0 \\ \frac{\phi \cdot P_1 (1-z)}{(z-(1-\alpha \cdot P_1))} & \frac{\beta \cdot P_2}{(z-(1-\beta \cdot P_2))} \end{bmatrix} \begin{bmatrix} U_1(z) \\ U_2(z) \end{bmatrix} \quad (12)$$

E. Control Law Reformulation

Looking at the transfer function for the realized dwell (Y_2), there is a zero at +1 relating the realized dwell to the commanded on time, u_1. This zero results in the observed overshoot. A new control law to replace Eq. 5 is proposed for the CDT state equation.

$$\begin{aligned} CDT(k+1) &= CDT(k) + P_2(RD_{des} - RD(k)) \quad (13) \\ &- \frac{\phi \cdot P_2}{\alpha} \cdot Q(k) \end{aligned}$$

The state space formulation with this new control law is shown below in Eq. 14.

$$\begin{bmatrix} x_1(k+1) \\ x_2(k+1) \end{bmatrix} = \begin{bmatrix} (1-P_1\alpha) & 0 \\ 0 & (1-P_2\beta) \end{bmatrix} \begin{bmatrix} x_1(k) \\ x_2(k) \end{bmatrix} + \begin{bmatrix} P_1 & 0 \\ 0 & P_2 \end{bmatrix} \begin{bmatrix} u_1(k) \\ u_2(k) \end{bmatrix} \quad (14)$$

The convenient diagonal structure of this new formulation is a result of the specifically chosen control law of Eq. 13. The new transfer function matrix formulated from Eq. 14 is shown below in Eq. 15.

$$\begin{bmatrix} Y_1(z) \\ Y_2(z) \end{bmatrix} = \begin{bmatrix} \frac{\alpha \cdot P_1}{(z-(1-\alpha \cdot P_1))} & 0 \\ \frac{-\phi \cdot P_1}{(z-(1-\alpha \cdot P_1))} & \frac{\beta \cdot P_2}{(z-(1-\beta \cdot P_2))} \end{bmatrix} \begin{bmatrix} U_1(z) \\ U_2(z) \end{bmatrix} \quad (15)$$

The zero has been eliminated with the new control law, however, it is necessary to check that the steady state error will be zero for both the desired pulse one quantity and the realized dwell, Q_{des} and RD_{des}, respectively. Utilizing the final value theorem,

$$\lim_{k \to \infty} Y(k) = \lim_{z \to 1} [(1-z^{-1})Y(z)]$$

and assuming a step input of both Q_{des} and RD_{des}, the following final values for Q and RD were found using the transfer functions from Eq. 15.

$$Q(\infty) = Q_{des}$$

$$RD(\infty) = -\frac{\phi}{\alpha} \cdot Q_{des} + RD_{des}$$

This implies that the steady-state error for realized dwell will not go to zero.

F. Final Control Law

While the pulse one quantity, Q, approaches the desired value, the realized dwell, RD, does not. This will require a reformulation of the control law to ensure zero steady-state error. A final control law for the CDT and the realized dwell is proposed.

$$\begin{aligned} CDT(k+1) &= CDT(k) + P_2(RD_{des} - RD(k)) \\ &+ \frac{\phi \cdot P_2}{\alpha}(Q_{des} - Q(k)) \quad (16) \end{aligned}$$

This results in the corresponding state space formulation

$$\begin{bmatrix} x_1(k+1) \\ x_2(k+1) \end{bmatrix} = \begin{bmatrix} (1-P_1\alpha) & 0 \\ 0 & (1-P_2\beta) \end{bmatrix} \begin{bmatrix} x_1(k) \\ x_2(k) \end{bmatrix} + \begin{bmatrix} P_1 & 0 \\ \frac{\phi \cdot P_2}{\alpha} & P_2 \end{bmatrix} \begin{bmatrix} u_1(k) \\ u_2(k) \end{bmatrix} \quad (17)$$

and the transfer function matrix

$$\begin{bmatrix} Y_1(z) \\ Y_2(z) \end{bmatrix} = \begin{bmatrix} \frac{\alpha \cdot P_1}{(z-(1-\alpha \cdot P_1))} & 0 \\ \frac{-\phi \cdot P_1}{(z-(1-\alpha \cdot P_1))} + \frac{\phi \cdot P_2 \cdot \beta}{(z-(1-\beta \cdot P_2))} & \frac{\beta \cdot P_2}{(z-(1-\beta \cdot P_2))} \end{bmatrix} \begin{bmatrix} U_1(z) \\ U_2(z) \end{bmatrix} \quad (18)$$

This "extended" control law also eliminates the zero effect like the previous control law. Next, the final value theorem is again utilized to check the steady-state error of both Q and RD.

$$Q(\infty) = Q_{des}$$

$$RD(\infty) = RD_{des}$$

This control law yields a system with real, positive eigenvalues, zero steady-state error, and no problematic zeros. The transient response of both pulse one quantity and realized dwell with the extended control law is shown below in Fig. 13 and 14 with eigenvalues at 0.9.

As desired, both transient responses show overdamped, asymptotic behavior reducing the likelihood of pulses-to-pulse bleeding and instability as described in Sect. V-C.

VI. CONCLUSIONS AND FUTURE WORK

A. CONCLUSIONS

This paper summarizes the utilization of a piezoelectric fuel injector flow rate estimation strategy for cycle-to-cycle

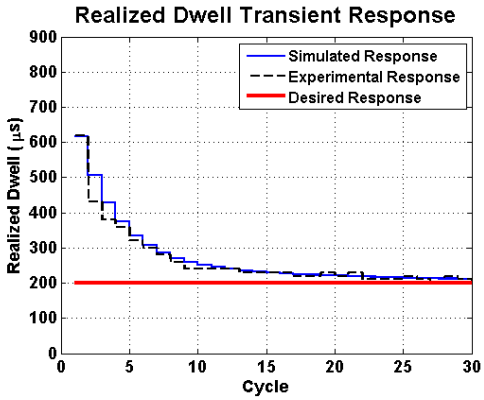

Fig. 13. Transient Response of Realized Dwell with Extended Controller

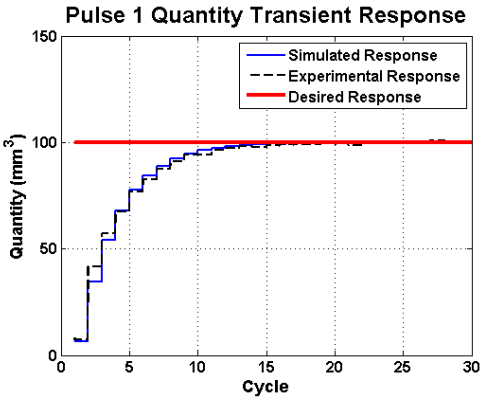

Fig. 14. Transient Response of Pulse One Quantity with Extended Controller

computation. High speed data acquisition captures and stores important estimation variables such as the stack voltage and body pressure during the injection period, and computation of state variables is delayed to more efficiently utilize the processor over the entire cycle. With this cycle-to-cycle estimation of flow being available as feedback, a preliminary controller was developed for control of quantities and realized dwell times for tightly spaced, multiple pulse profiles. A simplified "two pulse approximation" model is developed and coupled with a modified discrete integral controller, and with some reformulation, is shown to have no steady-state error and the required overdamped, asymptotic behavior to prevent pulse bleed during control action. Simulation and experimental data validates the control scheme for two pulses.

B. FUTURE WORK

Future work will involve analytical determine of the constants β, ϕ, and α as opposed to the empirical approximations used in this paper. Also, the control laws developed will be expanded to operate across varying rail pressures. The controller will also be validated for longer and more complex multiple pulse profiles.

REFERENCES

[1] D. Hareendranath, N. Gajarlawar, M. Manickam, and G. Pundlik, *Low End Performance Improvement by Effective Use of Multiple Injection Strategy in Common Rail Diesel Engine*. Milwaukee, Wisconsin, USA: Proceedings of the ASME Internal Combustion Engine Division 2009 Spring Technical Conference, 2009.

[2] S. Mendez and B. Thirouard, "Using multiple injection strategies in diesel combustion: Potential to improve emissions, noise and fuel economy trade-off in low cr engines," *SAE 2008-01-1329*, 2008.

[3] J. Lee, K. Min, K. Kang, and C. Bae, "Hydraulic simulation and experimentatal analysis of needle response and controlled injection rate shape characteristics in a piezo-driven diesel injector," *SAE 2006-01-1119*, 2006.

[4] C. Fettes and A. Leipertz, "Potentials of a piezo-driven passenger car common rail system to meet future emission legislations - an evaluation by means of in-cylinder analysis of injection and combustion," *SAE 2001-01-3499*, 2001.

[5] C. Satkoski and G. Shaver, "Piezoelectric fuel injection - pulse-to-pulse coupling and flow rate estimation," *IEEE/ASME Transactions on Mechatronics*, 2010.

[6] C. A. Satkoski, G. M. Shaver, R. More, P. Meckl, and D. Memering, "Dynamic modeling of a piezoelectric actuated fuel injector (in review)," *Journal of Dynamic Systems, Measurement, and Control*, 2009.

[7] W. Bosch, "Fuel rate indicator: a new measuring instrument for display of the characteristics of individual injection," *SAE 660749*, 1966.